ACS APPLIED MATERIALS & INTERFACES

Research Article

www.acsami.org

Dielectric Effects at Organic/Inorganic Interfaces in Nanostructured Devices

Tejas S. Sherkar* and L. Jan Anton Koster

Photophysics and Optoelectronics, Zernike Institute for Advanced Materials, University of Groningen, Nijenborgh 4, 9747AG Groningen, The Netherlands

ABSTRACT: Dielectric interfaces are important in organic electronic devices, as they dominate charge generation and recombination dynamics and set the tone for efficiency of the device. In a charge separation scenario across the interface, we calculate the binding energy of a charge carrier for variations in dielectric mismatch (i.e., the ratio of the dielectric constant of materials forming the interface), interface shape and size, and dielectric anisotropy. We find that dielectric mismatch results in binding of the charge carrier to the interface with energies on the order of several *kT*. For the variation in interface shape and size, epitomized by the device morphology, we show that the assumption of a planar interface overestimates the attractive potential. The change in the interface curvature affects the binding energy of the charge carrier by order of *kT*. Anisotropy is shown to affect critically the electric field along the principal axis, while the binding energy of the charge is altered by more than 5 *kT*. We are able to give an upper limit on the change in the binding energy for the variations in the above interfacial factors. These limits can serve as guidelines for optimization, interface engineering, and design of high efficiency organic electronic devices.

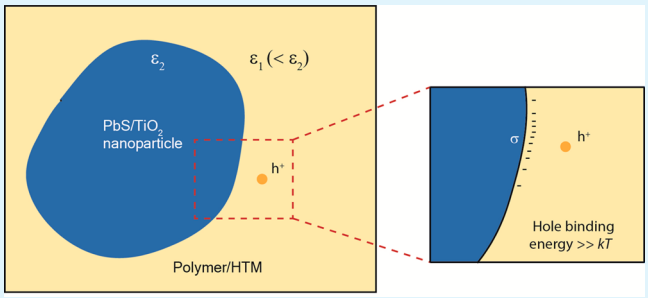

KEYWORDS: *dielectric, binding energy, curvature, anisotropy, organic, hybrid*

1. INTRODUCTION

Dielectric boundaries are ubiquitous in organic electronic devices that make use of heterojunction architectures. Interfaces between materials play a crucial role in the device performance, as they are active sites for charge generation and recombination.[1] For example, the interfaces present in organic and hybrid solar cells, multilayer organic light emitting diodes (OLEDs), and organic field effect transistors (OFETs). Although metal−dielectric interfaces at electrode contacts have been extensively studied and their effect on device performance explained by means of image potentials,[2,3] dielectric−dielectric interfaces in the active layer of the device remain disregarded. Recently, a few theoretical analyses have urged consideration of dielectric−dielectric interfaces in the context of organic electronic devices.[4,5] However, apart from the widely recognized feature of any dielectric interface, namely the dielectric mismatch (i.e., the ratio of the dielectric constant of materials), factors such as shape and size of the interface, and the anisotropy of the materials also govern the electrostatics near interfaces.

Electrostatic forces estimated by assuming the dielectric interface at electrode contacts to be planar can represent adequately the electrostatic effects near electrode contacts. However, a similar approach applied to dielectric boundaries in the active layer of a device would be an oversimplification. Dielectric boundaries in the active layer of a device are typically defined by the morphology and are complex in shape and size. Figure 1 shows the arbitrary nature of the interfaces realized in a dye sensitized solar cell (DSSC) after the sintering of TiO_2 nanoparticles.[6] Figure 2 shows various interface shapes and sizes resulting from the use of different nanoparticle shapes in a polymer/nanoparticle solar cell.[7] Likewise, anisotropy in materials forming the interface results in direction dependent response to an electric field and therefore needs to be realized in interfacial electrostatics. We show that these interfacial factors viz. dielectric mismatch, interface shape and size, and anisotropy contribute significantly to the interfacial electrostatics and stress their importance by studying their consequence in organic electronic devices.

According to the Maxwell−Wagner theory, charge accumulation occurs at interfaces between materials where a discontinuity in ε/σ occurs,[8] where ε is the dielectric constant and σ is the conductivity of the material. This accumulated charge (i.e., induced charge) is responsible for modification of the mesoscopic electric field distribution in the device. Fittingly, the dependence of the amount of accumulated charge on the interfacial factors such as dielectric mismatch, interface shape and size, and anisotropy needs to be realized in order to estimate the degree of modification of the electrostatics in a device.

Devices that make use of an organic/inorganic heterojunction (OI−HJ) as their charge-separating interface are of special interest, as they are characterized by high dielectric

Received: February 19, 2015
Accepted: May 20, 2015
Published: May 20, 2015

DOI: 10.1021/acsami.5b01606
ACS Appl. Mater. Interfaces 2015, 7, 11881−11889

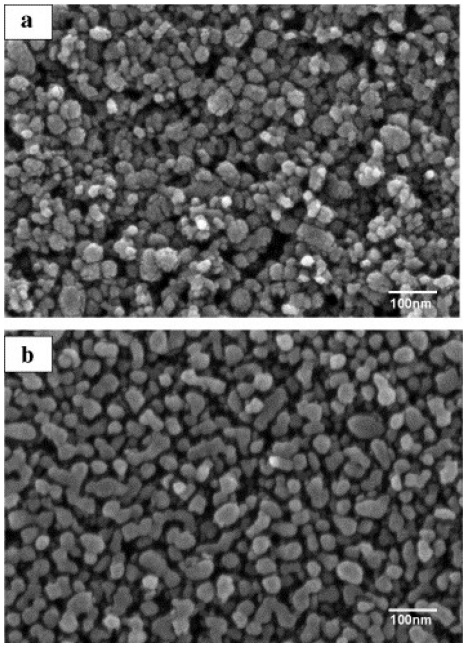

Figure 1. SEM images of surface views of (a) nonsintered and (b) sintered TiO_2 films in dye sensitized solar cells (DSSC).[6]

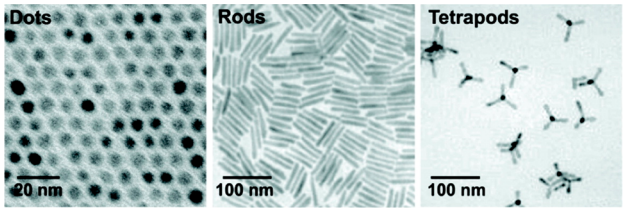

Figure 2. TEM images of nanoparticles of different geometry viz. dots, rods, and tetrapods used in organic−inorganic hybrid solar cells.[7]

mismatch ($\varepsilon_2/\varepsilon_1$) and a sharp dielectric discontinuity at the OI−HJ interface,[9] with the typical dielectric constant of organic materials (ε_1) being 1.5−4 and that of inorganic nanoparticles (ε_2) ∼10−100.[10] These devices include, but are not limited to, OI photodiodes,[11] dye sensitized solar cells (DSSCs),[12,13] colloidal quantum dot solar cells and light emitting devices,[14−16] and nanoparticle/organic solar cells.[17] Recent studies on charge dynamics at the OI−HJ in solid-state DSSCs[18,19] and nanoparticle/organic solar cells have attributed the low efficiency of these devices as compared to fully organic or inorganic devices to the poor charge separation and charge extraction efficiency.[20−23] Ten Cate et al. assigned the low mobility of charges near the nanoparticle/organic interface to the Coulomb force acting on the charges keeping them near the interface,[21] whereas Noone et al. discussed the increased lifetimes of charge carriers near the interface in context of increased charge screening by inorganic nanoparticles.[22] Although hypothesized to be the reason for modified charge dynamics near the interface, the extent of the dielectric mismatch needs to be investigated in detail.

As shown in Figures 1 and 2, the nanoparticle shape determines the morphology in a device. Recently, variation in nanoparticle shape was found to influence the local charge generation, separation, and therefore, the device performance.[24,25] However, the charge carriers interact with the local shape of the nanoparticle or more specifically the local curvature of the nanoparticle. This stimulates our study on the effect of the curvature of the dielectric interface on the electrostatic interactions between the charges. Additionally, the direction of the electric field across the interface was found to affect the charge separation dynamics,[26] which leads to our investigation on the effect of anisotropy on interfacial electrostatics.

In the context of organic photovoltaics, recent focus is on increasing the power conversion efficiency by increasing the dielectric constant of the active layer in organic photovoltaics.[27,28] This has led to synthesis of new materials having high dielectric constants[29,30] and introduction of high dielectric constant nanostructured materials in the active layer.[31] Therefore, as the dielectric constant of organic semiconductors is being realized as a central parameter for device performance, the physics of dielectric interfaces acquires new importance in trying to study the niceties leading to the device performance. Dielectric mismatch has been previously studied in optical analyses of organic heterojunctions using ellipsometry techniques.[32,33] However, at optical frequencies, the mismatch is greatly reduced due to lowering of the dielectric constants of the materials at high frequencies. This makes it viable to use an effective medium approximation (EMA) to describe mixtures of materials with known dielectric functions.[34,35]

In this paper, we show that the dielectric mismatch at interfaces affects the electrostatic interaction between the charge carriers and could be responsible for modified charge dynamics in nanostructured devices. For the purpose of calculations, arbitrary interfaces that are outlined by the complex morphology are considered to be made up of shapes that are symmetrical along one (plane) or two (cylinder) or three (sphere) axes or a combination of them. Charge carriers close to an interface thus experience electrostatic forces that can be calculated by summing up contributions from these abstract shapes making up the real morphology. We consider the case of dielectric mismatch at the OI−HJ in nanoparticle/organic solar cells and solid-state DSSCs. In a charge separation scenario across the interface, we calculate the binding energy of a charge carrier for variations in the dielectric mismatch ($\varepsilon_2/\varepsilon_1$), interface curvature, and anisotropy of the organic material. We show that the variation in the above interfacial factors results in change in the interaction energies of charges on the order of a few kT (=25.6 meV, at T = 298 K). Finally, we give an upper limit for the change in the binding energy for the variations in the above interfacial factors and issue guidelines for reduction of the dielectric effect at the end of the paper.

This paper is organized as follows: The theory for calculation of electrostatic forces in the presence of dielectric interfaces is described in section 2.1. Section 2.2 introduces two parameters to quantify the effect of dielectric inhomogeneity on the external charge distribution in a domain. Results and discussions are presented in section 3, with the effect of dielectric mismatch for planar interface calculated in section 3.1 and the effect of interface curvature and anisotropy of organic material investigated in section 3.2 and section 3.3 respectively. Conclusions are presented in section 4.

2. THEORY

We work within the continuum electrostatic model used to treat discrete charges in an inhomogeneous dielectric domain. The properties of different materials in the system are described in terms of bulk properties such as the average dielectric constant of the material.[36] Any dielectric boundary in the domain is assumed to be ideal having zero thickness. The external charges are considered to be

DOI: 10.1021/acsami.5b01606
ACS Appl. Mater. Interfaces 2015, 7, 11881−11889

point charges having unit magnitudes that polarize the surrounding dielectric.

2.1. Calculation of Electrostatic Forces. In a domain $\mathcal{D}$ with spatial variations of dielectric constant, the determination of the electrostatic forces on real charges involves solving the Poisson equation:

$$\nabla\cdot(\varepsilon(r)\nabla\Phi) = -\rho \tag{1}$$

with the electrostatic potential Φ, charge distribution ρ and spatially dependent permittivity $\varepsilon(r) = \varepsilon_0\varepsilon_{rel}(r)$, where $\varepsilon_{rel}(r)$ is the relative permittivity or the dielectric constant of the media. The solution to the above partial differential equation is subject to requirement of continuity of the electric potential (Φ) everywhere in the domain and to a suitable set of boundary conditions.[37] The choice of method used for solving the Poisson equation depends on the complexity of the problem at hand, which is typically determined by the dielectric distribution in the domain and the boundary conditions.

Many numerical methods exist to solve these partial differential equations, such as finite difference, finite element, or boundary element methods.[38] Among the widely popular finite difference methods, systems with sharp dielectric interfaces or discontinuous $\varepsilon(r)$ can be solved with increasing accuracy by the ghost fluid method (GFM),[39,40] the immersed interface method (IIM),[41] and the matched interface boundary (MIB) method.[42,43] Recent generalizations of MIB also take into account the arbitrary nature of interfaces including any geometric singularities.[44] See refs 38−44 for details.

Direct methods involve solving the Poisson equation in terms of the Green's function that satisfies $\Delta G(r - r') = -\delta(r - r')$, subject to the boundary conditions. These methods can be applied to systems with interfaces between different media having otherwise constant dielectric properties. The familiar image charge method can be used to account for the effect of planar interfaces between different isotropic media. The electrostatics in the presence of arbitrary shaped interfaces can be calculated via the induced charge computation (ICC*) method which self-consistently calculates the induced charges on the interface and is a boundary element method.[45]

Here, we briefly describe the image charge and the ICC* methods that are essential for our calculations to estimate the electrostatic interactions in systems having dielectric interfaces such as nanostructured hybrid organic/inorganic devices.

Image Charge. The physically intuitive solution for the Green's function for a system involving a point charge q in a dielectric medium ($\varepsilon = \varepsilon_1$) and placed at a distance $x = a$ from an interface with a metal ($\varepsilon = \infty$) involves replacing the metal with a virtual charge $-q$ at distance $x = -a$ from the interface on the other side,[37] as shown in Figure 3a.

However, the method of image charges is not limited to infinite mismatch as in the case of a metal−dielectric interface. If the metal is replaced by a finite dielectric ($\varepsilon = \varepsilon_2$), the system can be solved by taking into account the boundary conditions at the interface. The boundary condition at the interface requires the normal component of the electric flux density ($\mathbf{D}$) to be continuous across the dielectric interface B. In other words:

$$\mathbf{D}_{1n} = \mathbf{D}_{2n} \tag{2}$$

$$\varepsilon_1\mathbf{E}_{1n} = \varepsilon_2\mathbf{E}_{2n} \tag{3}$$

Equation 3 follows from eq 2 because the electric flux density is related to the electric field strength ($\mathbf{E}$) by $\mathbf{D} = \varepsilon\mathbf{E}$ assuming isotropic media.[37]

As shown in Figure 3b, the equivalent system to calculate the electrostatic contribution due of polarization of the two media involves considering two fictitious charges, where the first charge q' is placed at $x = -a$ from the interface and the second charge q'' at $x = a$ from the interface.[37] The magnitudes of the image charges are given by

$$q' = (\varepsilon_1 - \varepsilon_2)/(\varepsilon_1 + \varepsilon_2)q \tag{4}$$

$$q'' = 2\varepsilon_1/(\varepsilon_1 + \varepsilon_2)q \tag{5}$$

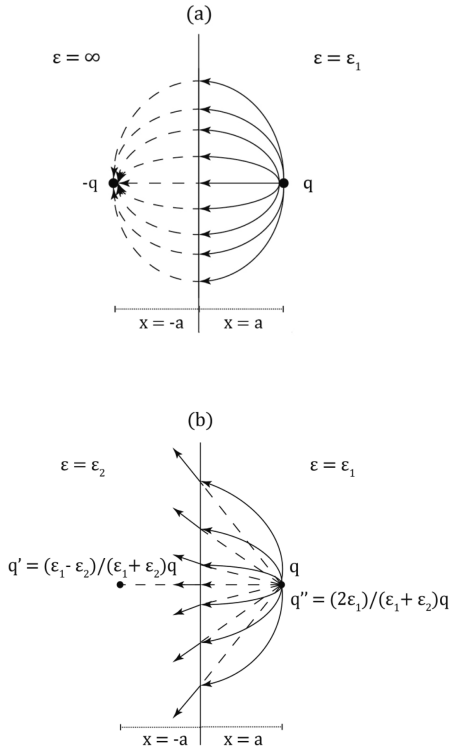

Figure 3. Solution to the Poisson equation with a point charge placed at a distance $x = a$ from (a) a metal−dielectric interface and (b) a dielectric−dielectric interface. The lines drawn in the figures are the electric field lines originating from the actual charge.

The electrostatic potential and the electric field is then calculated in a uniform dielectric medium $\varepsilon = \varepsilon_1$ and replacing medium $\varepsilon = \varepsilon_2$ with image charges q' and q''.

Induced Charge Computation (ICC).* This boundary element method involves replacing the inhomogeneity in the system by an equivalent uniform dielectric with appropriate surface charges σ at the interface where the dielectric constant has a discontinuity. The surface charge can be calculated from the relation:[45]

$$(\mathbf{E}_1 - \mathbf{E}_2)\cdot\mathbf{n} = \sigma/\varepsilon_1 \tag{6}$$

where $\mathbf{E}$ is the electric field at the interface, $\mathbf{n}$ is the outward unit normal. Equation 6 follows from the discontinuity in the normal component of $\mathbf{E}$ at the dielectric interface, which is replaced by the surface charge.

As shown in Figure 4, the interface B is divided into N small elements located at $\mathbf{x}_i$ and the charge on each element is calculated iteratively by using the linear relation between $\mathbf{E}$ and σ viz. eq 6 until convergence.

$$\sigma_i = f\mathbf{E}_i\cdot\mathbf{n}_i \tag{7}$$

In eq 7, $f = (\varepsilon_1/2\pi)(\varepsilon_1 - \varepsilon_2)/(\varepsilon_1 + \varepsilon_2)$ is the permittivity dependent factor.[45] The electric field $\mathbf{E}_i$ is due to all charges (external and induced) but the one induced at location $\mathbf{x}_i$. The electrostatic potential in the system is then calculated by summing up Coulomb potentials due to both, the external charges as well as the surface induced charge σ in a domain with homogeneous permittivity ε_1.

Although the image charge method can be applied to problems limited to simple geometric interfaces, the induced charge computation method can be applied to systems where interfaces are arbitrary in number, shape, and have large dielectric mismatch. Therefore, the ICC* method is most suited for our calculations.

2.2. Characterization. To quantify the effect due to dielectric inhomogeneity in the domain, we introduce two parameters that denote the contribution of the dielectric interface to the electrostatic energy of external charges and the electrostatic force experienced by

DOI: 10.1021/acsami.5b01606
ACS Appl. Mater. Interfaces 2015, 7, 11881−11889

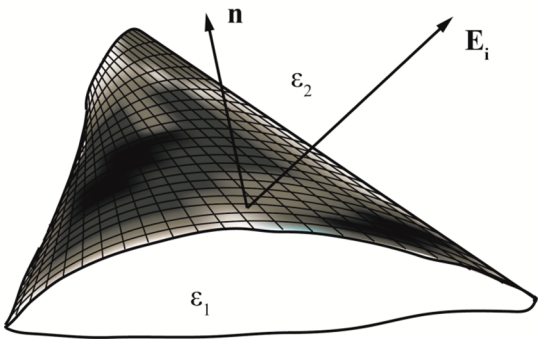

Figure 4. Discretization of the interface between two regions of permittivity ε_1 and ε_2 into small elements. The induced surface charge is calculated on each element from eq 7.

them. Consider a system with q_i (i = 1, 2, ... N) external charges and a dielectric boundary B. The induced surface charge density on B due to polarization is σ.

Dielectric Binding Energy (BE^{diel}). If the electrostatic potential at charge q_i due to the induced charge σ is V_i^{diel}, the dielectric binding energy (or equivalently termed as the dielectric contribution to the binding energy) of q_i is

$$BE_i^{diel} = q_i V_i^{diel} \tag{8}$$

And the relative dielectric contribution to the interaction energy between external charges q_i and q_j is

$$BE_{ij}^{diel} = q_i q_j (V_i^{diel} - V_j^{diel}) \tag{9}$$

Dielectric Electric Field ($\mathbf{E}^{diel}$). The electric field at the location of external charge q_i due to induced surface charge σ is the dielectric electric field $\mathbf{E}_i^{diel}$. Although BE^{diel} solely is able to quantify the effect of dielectric inhomogeneity on external charges, we find that in cases where anisotropy exists, $\mathbf{E}^{diel}$ is a more useful parameter.

For example, if a charge is kept near a dielectric interface, the BE^{diel} denotes the energy required to move the charge away from the interface to infinity (at zero potential). Similarly, $\mathbf{E}^{diel}$ denotes the electric field force experienced by the charge due to the dielectric boundary.

3. RESULTS AND DISCUSSION

In our calculations, we consider the case of dielectric mismatch at the OI−HJ in nanoparticle/organic solar cells and solid-state DSSCs that make use of photoactive inorganic nanoparticles like PbS,[21] CdSe,[17] TiO_2,[12] and organic materials like P3HT,[21] PCBM,[21] and Spiro-OMeTAD.[13] In these devices, light absorption by a nanoparticle results in a photoexcited charge pair of electron and hole that is separated across the nanoparticle/organic interface.[46] We consider the situation in which the electron is localized on the nanoparticle and the hole in the organic semiconductor. Because the mobility of the electron in the nanoparticle is high as compared to the mobility of hole in the hole transport material,[47] we consider the charge separation scenario where the electron quickly moves away from the nanoparticle/organic interface[20] and the hole experiences full electrostatic effects from the induced charges due to polarization.

The organic material is assumed to uniformly wet the nanoparticle in space and the interface is defined by a sudden jump in dielectric constant from the organic material with a bulk relative permittivity of ε_1 = 3 to the inorganic nanoparticle with bulk relative permittivity range ε_2 = 10−100. For estimating the effect of the change in dielectric mismatch $(\varepsilon_2/\varepsilon_1)$ on the binding energy of the hole, the dielectric constant organic material is kept constant at ε_1 = 3 and that of the inorganic nanoparticle (ε_2) is varied in a suitable range.

The bulk dielectric constant underestimates the electrostatic interaction for very small distances. A distance dependent dielectric constant function $\varepsilon(r)$ can be introduced[48]

$$\varepsilon(r) = \varepsilon_s - (\varepsilon_s - 1)\left(1 + sr + \frac{1}{2}s^2r^2\right)e^{-sr} \tag{10}$$

where the parameter s is the inverse screening length and is set at 3 nm^{-1} for disordered organic semiconductors.[49] Thus, for distances below 1 nm, the bulk dielectric constant is not capable of describing the polarization effects. Then a dielectric gradient can be said to exist between r = 0 and r = 1 nm. Incorporation of dielectric gradient in currently outside the scope of our analysis. We henceforth focus on distances above 1 nm for the charge from the interface.

3.1. Planar Dielectric Interface. The electrostatic force experienced by a charge in dielectric medium $(\varepsilon = \varepsilon_1)$ placed at a distance $x = a$ from a planar dielectric interface formed with another dielectric medium $(\varepsilon = \varepsilon_2)$ is calculated by the image charge method explained in section 2.1. The magnitude and sign of the image charges q' and q'' as shown in Figure 3b depend on the ratio $\varepsilon_2/\varepsilon_1$. The electric field at the location of the original charge is due to the image charge $q' = (\varepsilon_1 - \varepsilon_2)/(\varepsilon_1 + \varepsilon_2)q$ at $x = -a$ and is given by

$$\mathbf{E} = \left(\frac{\varepsilon_1 - \varepsilon_2}{\varepsilon_1 + \varepsilon_2}\right)\frac{q}{4\pi\varepsilon_0\varepsilon_1(2a)^2} \tag{11}$$

where ε_0 is the vacuum permittivity. From eq 11, it is evident that if $\varepsilon_1 < \varepsilon_2$, the electric field experienced by the original charge is attractive in nature, irrespective of its sign. In essence, a charge near a high dielectric object has a natural tendency to drift toward the interface. This Coulomb attraction clarifies the literature suggested premises of trapping of charge carriers near the interfaces in devices.[22,50] Similarly, a charge in a dielectric medium close to an interface with air $(\varepsilon = 1)$ would experience a repulsive force irrespective of its sign. The charge would thus have a propensity to move away from the surface (dielectric−air interface) and stay in the bulk of the dielectric medium.

The dielectric binding energy BE^{diel} then represents the energy required to unpin or move the charge to infinity. The scale of this required energy can be seen in Figure 5, which shows the variation in binding energy with dielectric mismatch $(\varepsilon_{2/}\varepsilon_1)$ for a charge placed at a distance of x = 1 to x = 5 nm from the dielectric interface.

In short, high dielectric mismatch is unfavorable for efficient separation of charges from the interface. The mismatch results in an external energy requisite upward of several kT in order for the pinned charges to separate from the interface. This energy is generally provided by the external electric field set by the difference in the work function of the contacts or the energy offset in the LUMO−LUMO energy levels of the materials forming the interface. If the requirement of this external energy were to decrease, higher open circuit voltages (V_{OC}) can be realized by tuning the LUMO levels of the materials.[51,52]

3.2. Effect of Interface Curvature. Here, we consider the dielectric mismatch across the nanoparticle/organic interface and calculate the effect of nanoparticle curvature on the binding energy of a hole (+e) in the organic material near the interface.

As shown in Figure 6a−c, the hole is located on the x-axis at a distance x nm from the interface. The three-dimensional local

DOI: 10.1021/acsami.5b01606
ACS Appl. Mater. Interfaces 2015, 7, 11881−11889

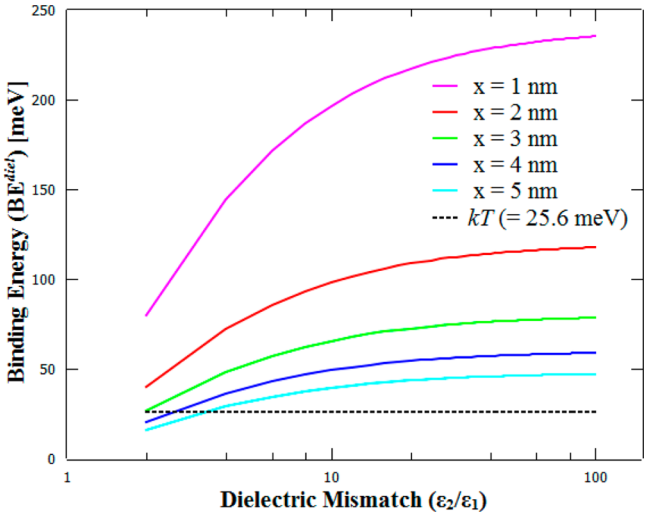

Figure 5. Plot of variation of binding energy (BE^{diel} in units of meV) with dielectric mismatch ($\varepsilon_2/\varepsilon_1$). The five different plots represent different distance between the hole and the dielectric interface.

interface curvature is denoted by R_X, R_Y, and R_Z in x, y, and z directions, respectively. The curvature is varied from spherical ($R_X = R_Y = R_Z = 1/5\ nm^{-1}$) to cylindrical ($R_X = R_Z = 1/5\ nm^{-1}$, $R_Y = 0$) to planar ($R_X = R_Y = R_Z = 0$). The typical values of the nanoparticle interface curvature considered are taken from the literature.[22] The dielectric contribution to the binding energy of the hole is calculated for all three interfaces and the comparison is shown in Figure 7.

As is evident from Figure 7, the binding energy of the hole near a planar interface is higher than in the case of cylindrical and spherical interface. The increase in the binding energy of hole in going from a spherical to a planar interface can be attributed to increase in the magnitude of induced charge on the interface. From eq 5, the magnitude of the induced charge depends on the strength of the electric field and the angle (θ) between the surface normal of the induced charge area on the interface and the direction of the electric field.

$$\sigma_i = f\mathbf{E}_i\mathbf{n}_i\cos\theta \tag{12}$$

The product $\mathbf{E}_i\cos\theta$ increases with dimensionality from spherical to cylindrical to planar, leading to increase in the magnitude of the induced charge. This increased induced charge is responsible for the higher binding energy of the hole.

The spherical and cylindrical curvature described above can be said be convex in nature. Following the trend shown in Figure 7, the binding energy for a concave interface ($R_X = R_Y = R_Z = -1/5\ nm^{-1}$) will be higher as compared to the convex interface. Figure 8 shows the comparison between the binding energy of the hole for a convex spherical, a planar and a concave spherical interface. Clearly, concave interfaces lead to stronger binding of charges at interfaces as compared to convex interfaces.

From the magnitude of the binding energies in Figure 7, it is evident that the hole experiences strong attraction from the induced charge on the interface. This is in conjunction with conclusions made from recent experimental findings[20−22] that showed decreased charge mobility and increased carrier lifetimes near the nanoparticle/organic interface. The presence of high dielectric mismatch in hybrid solar cells as compared with fully organic or inorganic solar cells could be one of the reasons for their poor power efficiency.

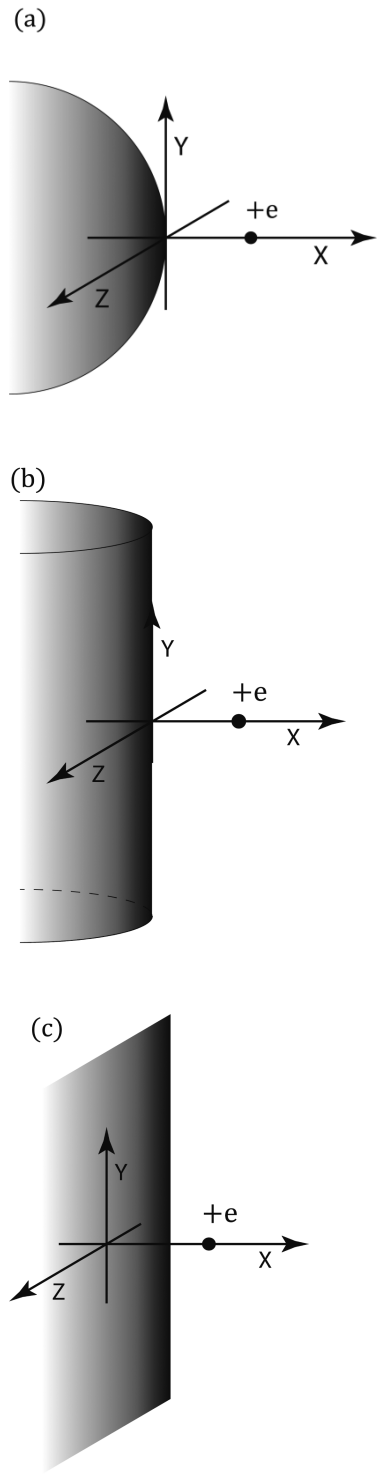

Figure 6. Schematic of different interface curvatures (a) spherical, (b) cylindrical, and (c) planar and their orientation with respect to the position of the hole (+e) on the x-axis.

It is noteworthy that the change in the interface curvature (defined by the local shape and size) affects the binding energy of the hole by order of kT. Hence, the assumption of a planar interface for estimation of electrostatic forces would be a limitation for systems involving arbitrary dielectric interfaces. The effect of the interfaces described by the complex morphology can then can be calculated by accounting the

DOI: 10.1021/acsami.5b01606
ACS Appl. Mater. Interfaces 2015, 7, 11881−11889

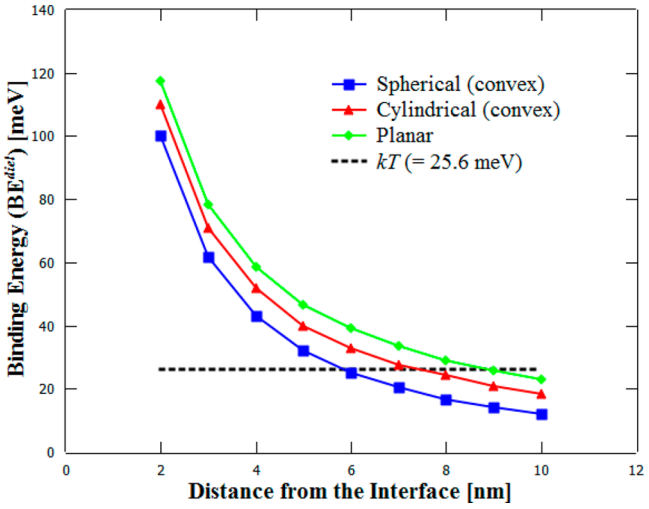

Figure 7. Variation of binding energy (BE^{diel} in units of meV) of the hole with distance (x in nm) from the nanoparticle/organic interface. The figure compares BE^{diel} of hole near a convex spherical (blue), a convex cylindrical (red), and a planar (green) interface.

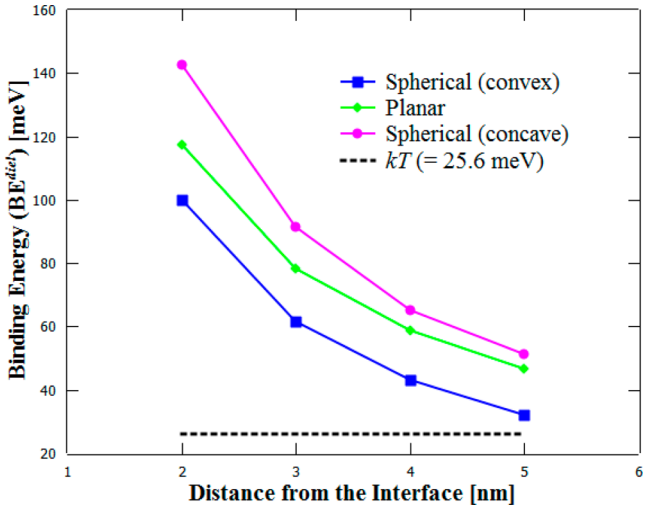

Figure 8. Variation of binding energy (BE^{diel} in units of meV) of the hole with distance (x in nm) from the nanoparticle/organic interface for a hole near a convex spherical (blue), a planar (green) and a concave spherical (magenta) interface. Lines are drawn to guide the eye.

electrostatic contributions from these abstract shapes making up the morphology.

3.3. Effect of Dielectric Anisotropy. In organic materials, the anisotropic nature of the polar molecules and their packing determines the spatial dependency of the dielectric constant on the mesoscopic scale. Anisotropic dielectric materials show directionally dependent polarizability and hence influence external charges present in the materials differently in different directions. With charge separation across the nanoparticle/organic interface sensitive to the direction of the electric field,[26] we are curious to determine the effect of dielectric mismatch at an interface present between an anisotropic organic material and an isotopic inorganic material.

We consider a planar interface at $x = 0$ between the isotropic inorganic material ($x < 0$) and anisotropic organic material ($x > 0$) with a hole placed on the x-axis in the organic material close to the interface. The isotropic dielectric constant of the inorganic material is $\varepsilon_2 = 100$, whereas the anisotropic dielectric constant of the organic material is expressed as a tensor:

$$\varepsilon_1 = \begin{pmatrix} \varepsilon_x & 0 & 0 \\ 0 & \varepsilon_y & 0 \\ 0 & 0 & \varepsilon_z \end{pmatrix} \sim \{\varepsilon_x, \varepsilon_y, \varepsilon_z\} \tag{13}$$

where ε_x, ε_y, and ε_z are dielectric constants in x, y, and z directions, respectively. The estimation of induced charge on the interface involves solving eq 7 iteratively with the product $f^* \mathbf{E}_i$ calculated independently in x, y, and z directions.

$$\sigma_i = (f_x(\mathbf{E}_i)_x + f_y(\mathbf{E}_i)_y + f_z(\mathbf{E}_i)_z)\cdot\mathbf{n}_i \tag{14}$$

where

$$f_x = \frac{\varepsilon_{1x}}{2\pi}\left(\frac{\varepsilon_{1x} - \varepsilon_2}{\varepsilon_{1x} - \varepsilon_2}\right) \tag{15}$$

$$f_y = \frac{\varepsilon_{1y}}{2\pi}\left(\frac{\varepsilon_{1y} - \varepsilon_2}{\varepsilon_{1y} - \varepsilon_2}\right) \tag{16}$$

$$f_z = \frac{\varepsilon_{1z}}{2\pi}\left(\frac{\varepsilon_{1z} - \varepsilon_2}{\varepsilon_{1z} - \varepsilon_2}\right) \tag{17}$$

The electrostatic potential and electric field in the domain is calculated by summing up contributions from the hole and the induced charges on the interface. Figure 9 shows the comparison of the binding energy (BE^{diel}) of the hole and the electric field ($\mathbf{E}^{diel}$) at the hole position with distance for cases: (1) isotropic $\varepsilon_1 = \{3,3,3\}$, (2) anisotropic in x direction $\varepsilon_1 = \{1,3,3\}$, and (3) anisotropic in y direction $\varepsilon_1 = \{3,1,3\}$ (the interface is symmetric in y and z directions).

From Figure 9a, the change in binding energy in going from the isotropic case to the anisotropic case in the x direction is more than the change in binding energy in going from the isotropic case to the anisotropic case in the y (or z) direction. The direction dependent effect of anisotropy on the binding energy of the hole can be explored by considering the electric field at the location of the hole. From Figure 9b, anisotropy in the y direction results in no change in the magnitude of the electric field, whereas anisotropy in the x direction leads to lowering of the electric field experienced by the hole. This is due to modification in the amount of induced charge on the interface in case 2 viz. when anisotropy exists in the x direction (principal axis). Hence, although the effective dielectric constant of the organic medium in case 2 and 3 is identical, the increase of the surface induced charge in case 2 results in increased BE^{diel}. Whereas, the electric field being a vector and its components being independently proportional to the dielectric constant in component directions results in its same magnitude for cases 1 and 3.

Anisotropy in the principal axis of other symmetric nature of interfaces (spherical, cylindrical, etc.) would result in a similar effect on the binding energy of the hole placed close to the interface. Thus, the effect of anisotropy in materials forming an interface with another material depends on the anisotropic tensor in three dimensions and the arbitrary nature of the interface including its shape and size.

These calculations indicate that dielectric mismatch in organic electronic devices results in binding of charge carriers at the interface with the energy required for effective charge

DOI: 10.1021/acsami.5b01606
ACS Appl. Mater. Interfaces 2015, 7, 11881−11889

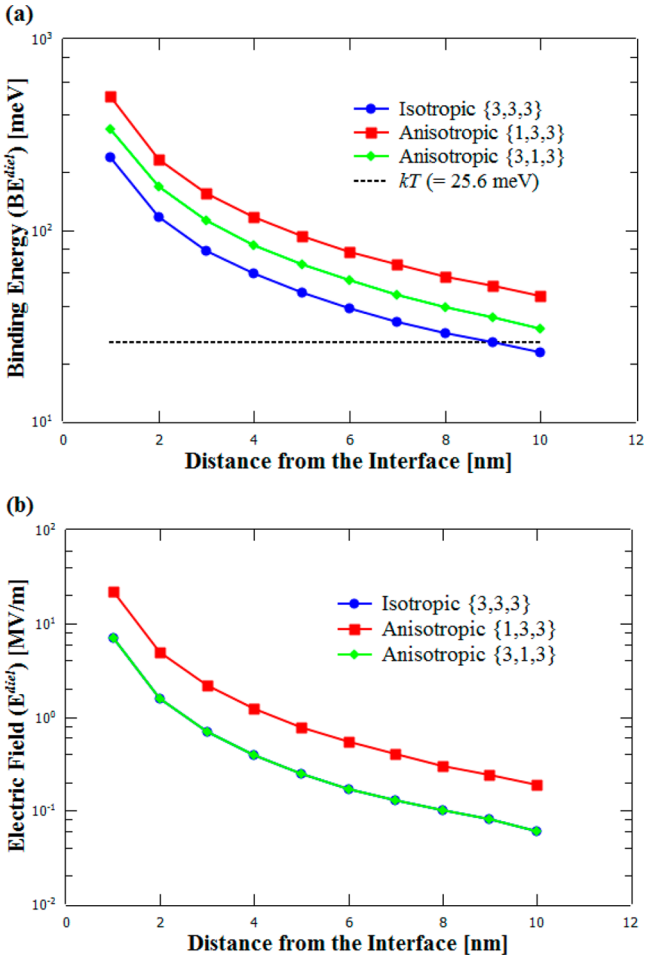

Figure 9. Comparison of variation in (a) binding energy (BE^{diel} in meV) of the hole and (b) electric field ($\mathbf{E}^{diel}$ in MV/m) with distance (in nm) for cases: (1) isotropic in *x*, *y*, and *z* direction (blue), (2) anisotropic in *x* direction (red), and (3) anisotropic in *y* direction (green).

separation up to several *kT*. This is also in conjunction with the literature where dielectric mismatch leads to pinning of charges at the interface.[50] The Coulomb attraction between the charge carrier and the induced charge on the interface would restrain the natural transport away from the interface, which overlaps with conclusions made from recent experimental findings[20−22] that showed decreased charge mobility and increased carrier lifetimes near the nanoparticle/organic interface. A large dielectric mismatch should thus be avoided as the binding energy of the charge carrier is found to increase with increase in dielectric mismatch. Although incorporation of inorganic nanostructures offers the possibility for plasmon enhanced effects and higher absorption in the active layer of a device,[53−55] the dielectric mismatch introduced by adding these inorganic nanostructures could act as an inhibitor for efficient charge separation in the device. The mismatch can be lowered by coating the nanoparticle with a low dielectric material,[56] which also leads to passivation of surface states and slowing down of interfacial charge transfer rate.[57] A close inspection of charge dynamics in such a system is thus required in order to quantify the effect due to lowering of the dielectric mismatch.

Change in the interface curvature also influences the Coulomb attraction experienced by the charge carrier with binding energy affected by order of *kT*. A charge near a convex spherical interface can be said to have a lower chance of recombination as compared to a similar charge near a cylindrical or planar interface. This follows the conclusions from recent studies, where variation in nanoparticle shape was found to influence the charge separation and consequently the device performance.[24,25] Any complex morphology can be considered to be made up of abstract shapes viz. a sphere, a cylinder, and a plane. The electrostatic contributions from these shapes can then be accounted for in order to estimate the electrostatic forces due to the interfaces resulting from the actual morphology.

It is also noteworthy that anisotropy along the principal axis of the interface results in a change in the binding energy of the charge by several *kT* as compared to the isotropic case. The electric field, particularly, is found to be critically affected by anisotropy due to change in the amount of induced charge on the interface.

4. CONCLUSIONS

In conclusion, we computed the electrostatic interactions between external charges in the presence of dielectric interfaces and demonstrated the importance of taking the dielectric mismatch into consideration in the context of organic electronic devices. We showed that high dielectric mismatch is responsible for binding of the charge carrier near the interface with energies above several *kT*. Dielectric mismatch is unfavorable for efficient separation of charge and should be avoided in the active layer of a device. Consideration of the large dielectric mismatch, which is typical of hybrid organic/inorganic devices, can help to understand the low mobility of charge carriers near the interface and also explain the high charge recombination at interfaces observed in the literature. For the variation in interface shape and size (both defined by the morphology), we showed that assumption of the planar interface overestimates the attractive potential. The change in the interface curvature (defined by the local shape and size) was found to affect the binding energy of the charge carrier by order of *kT*. The electrostatic forces in any complex morphology can be estimated by accounting for the contributions from the abstract shapes of interfaces viz. a sphere, a cylinder, and a plane that outline the real morphology. Optimization of morphology to avoid planar or concave interfaces would lower the binding of charge carriers at the interface. In the case of anisotropy in the organic material, we showed that it critically affects the electrostatic force along the principal axis and results in change in the binding energy of the charge by more than 5 *kT*. The contribution of anisotropy in charge dynamics is therefore not to be neglected.

The values stated above can be considered as upper limits to the change in the binding energy for the variations in the interfacial factors. For device optimization, following guidelines should be taken into consideration: (1) avoid large dielectric mismatch in the active layer by suitable choice of materials, (2) avoid planar and concave interfaces by optimization of morphology, and (3) ensure isotropic surrounding near interfaces by controlled processing and fabrication techniques.

AUTHOR INFORMATION

Corresponding Author

*Tejas S. Sherkar. E-mail: t.sherkar@rug.nl.

DOI: 10.1021/acsami.5b01606
ACS Appl. Mater. Interfaces 2015, 7, 11881−11889

Author Contributions

The paper was written through contributions of all authors. All authors have given approval to the final version of the paper.

Notes

The authors declare no competing financial interest.

■ ACKNOWLEDGMENTS

This work is part of the Industrial Partnership Programme (IPP) "Computational sciences for energy research" of the Foundation for Fundamental Research on Matter (FOM), which is part of the Netherlands Organisation for Scientific Research (NWO). This research programme is cofinanced by Shell Global Solutions International B.V.

■ REFERENCES

(1) Koch, N. Organic Electronic Devices and Their Functional Interfaces. *ChemPhysChem* **2007**, *8*, 1438−1455.
(2) Scott, J. C. Metal-Organic Interface and Charge Injection in Organic Electronic Devices. *J. Vac. Sci. Technol., A* **2003**, *21*, 521.
(3) Twarowski, A. J. Energy Level Bending at Molecular Crystal Surfaces. *J. Chem. Phys.* **1982**, *77*, 1458.
(4) Szmytkowski, J. Analysis of the Image Force Effects on the Recombination at the Donor-Acceptor Interface in Organic Bulk Heterojunction Solar Cells. *Chem. Phys. Lett.* **2009**, *470*, 123−125.
(5) Schott, M. A Note on Image Potentials at Dielectric Interfaces and Their Possible Relevance in Organic Electronics. *Synth. Met.* **2013**, *184*, 48−51.
(6) Karthikeyan, C. S.; Thelakkat, M.; Willert-Porada, M. Different Mesoporous Titania Films for Solid-State Dye Sensitised Solar Cells. *Thin Solid Films.* **2006**, *511−512*, 187−194.
(7) Smith, A. M.; Nie, S. Semiconductor Nanocrystals: Structure, Properties, and Band Gap Engineering. *Acc. Chem. Res.* **2010**, *43*, 190−200.
(8) Weis, M.; Lin, J.; Taguchi, D.; Manaka, T.; Iwanoto, M. The Charge Transport in Organic Field-effect Transistor as an Interface Charge Propagation: The Maxwell-Wagner Effect Model and Transmission Line Approximation. *Jpn. J. Appl. Phys.* **2010**, *49*, 071603.
(9) Reenshaw, C. K.; Forrest, S. R. Excited State and Charge Dynamics of Hybrid Organic/Inorganic Heterojunctions. I. Theory. *Phys. Rev. B* **2014**, *90*, 045302.
(10) Zang, D. Y.; So, F. F.; Forrest, S. R. Giant Anisotropies in the Dielectric Properties of Quasi-Epitaxial Crystalline Organic Semiconductor Thin Films. *Appl. Phys. Lett.* **1991**, *59*, 823.
(11) So, F. F.; Forrest, S. R. Organic-on-Inorganic Semiconductor Photodetector. *IEEE Trans. Electron Devices* **1989**, *36*, 66−69.
(12) Vlachopoulos, N.; Liska, P.; Augustynski, J.; Graetzel, M. Very Efficient Visible Light Energy Harvesting and Conversion by Spectral Sensitization of High Surface Area Polycrystalline Titanium Dioxide Films. *J. Am. Chem. Soc.* **1988**, *110*, 1216−1220.
(13) Hagfeldt, A.; Boschloo, G.; Sun, L.; Kloo, L.; Pettersson, H. Dye-Sensitized Solar Cells. *Chem. Rev.* **2010**, *110*, 6595−6663.
(14) Sargent, E. H. Colloidal Quantum Dot Solar Cells. *Nat. Photonics.* **2012**, *6*, 133−135.
(15) McDonald, S. A.; Konstantatos, G.; Zhang, S.; Cyr, P. W.; Klem, E. J. D.; Levina, L.; Sargent, E. H. Solution-Processed PbS Quantum Dot Infrared Photodetectors and Photovoltaics. *Nat. Mater.* **2005**, *4*, 138−142.
(16) Coe-Sullivan, S.; Woo, W.-K.; Steckel, J. S.; Bawendi, M.; Bulović, V. Tuning the Performance of Hybrid Organic/Inorganic Quantum Dot Light-Emitting Devices. *Org. Electron.* **2003**, *4*, 123−130.
(17) Huynh, W. U.; Dittmer, J. J.; Alivisatos, A. P. Hybrid Nanorod-Polymer Solar Cells. *Science* **2002**, *295*, 2425−2427.
(18) Burschka, J.; Dualeh, A.; Kessler, F.; Baranoff, E.; Cevey-Ha, N.-L.; Yi, C.; Nazeeruddin, M. K.; Grätzel, M. Tris(2-(1H-pyrazol-1-yl)pyridine)cobalt(III) as p-Type Dopant for Organic Semiconductors and its Application in Highly Efficient Solid-State Dye-Sensitized Solar Cells. *J. Am. Chem. Soc.* **2011**, *133*, 18042−18045.
(19) Hardin, B. E.; Snaith, H. J.; McGehee, M. D. The Renaissance of Dye-Sensitized Solar Cells. *Nat. Photonics* **2012**, *6*, 162−169.
(20) Meister, M.; Baumeier, B.; Pschirer, N.; Sens, R.; Bruder, I.; Laquai, F.; Andrienko, D.; Howard, I. A. Observing Charge Dynamics in Surface Reactions by Time-Resolved Stark Effects. *J. Phys. Chem. C* **2013**, *117*, 9171−9177.
(21) Ten Cate, S.; Schins, J. M.; Siebbeles, L. D. A. Origin of Low Sensitizing Efficiency of Quantum Dots in Organic Solar Cells. *ACS Nano* **2012**, *6*, 8983−8988.
(22) Noone, K. M.; Subramaniyan, S.; Zhang, Q.; Cao, G.; Jenekhe, S. A.; Ginger, D. S. Photoinduced Charge Transfer and Polaron Dynamics in Polymer and Hybrid Photovoltaic Thin Films: Organic vs Inorganic Acceptors. *J. Phys. Chem. C* **2011**, *115*, 24403−24410.
(23) Graetzel, M.; Janssen, R. a J.; Mitzi, D. B.; Sargent, E. H. Materials Interface Engineering for Solution-Processed Photovoltaics. *Nature* **2012**, *488*, 304−312.
(24) Dayal, S.; Reese, M. O.; Ferguson, A. J.; Ginley, D. S.; Rumbles, G.; Kopidakis, N. The Effect of Nanoparticle Shape on the Photocarrier Dynamics and Photovoltaic Device Performance of Poly(3-hexylthiophene):CdSe Nanoparticle Bulk Heterojunction Solar Cells. *Adv. Funct. Mater.* **2010**, *20*, 2629−2635.
(25) Li, Z.; Wang, W.; Greenham, N. C.; McNeill, C. R. Influence of Nanoparticle Shape on Charge Transport and Recombination in Polymer/Nanocrystal Solar Cells. *Phys. Chem. Chem. Phys.* **2014**, *16*, 25684−25693.
(26) Wang, Y.; Liu, K.; Mukherjee, P.; Hines, D. A.; Santra, P.; Shen, H. Y.; Kamat, P.; Waldeck, D. H. Driving Charge Separation for Hybrid Solar Cells: Photo-Induced Hole Transfer in Conjugated Copolymer and Semiconductor Nanoparticle Assemblies. *Phys. Chem. Chem. Phys.* **2014**, *16*, 5066−5070.
(27) Koster, L. J. A.; Shaheen, S. E.; Hummelen, J. C. Pathways to a New Efficiency Regime for Organic Solar Cells. *Adv. Energy Mater.* **2012**, *2*, 1246−1253.
(28) Torabi, S.; Jahani, F.; Van Severen, I.; Kanimozhi, C.; Patil, S.; Havenith, R. W. A.; Chiechi, R. C.; Lutsen, L.; Vanderzande, D. J. M.; Cleij, T. J.; Hummelen, J. C.; Koster, L. J. A. Strategy for Enhancing the Dielectric Constant of Organic Semiconductors Without Sacrificing Charge Carrier Mobility and Solubility. *Adv. Funct. Mater.* **2014**, *1*, 150−157.
(29) Jahani, F.; Torabi, S.; Chiechi, R. C.; Koster, L. J. A.; Hummelen, J. C. Fullerene Derivatives with Increased Dielectric Constants. *Chem. Commun.* **2014**, *50*, 10645−10647.
(30) Cho, N.; Schlenker, C. W.; Knesting, K. M.; Koelsch, P.; Yip, H.-L.; Ginger, D. S.; Jen, A. K.-Y. High-Dielectric Constant Side-Chain Polymers Show Reduced Non-Geminate Recombination in Heterojunction Solar Cells. *Adv. Energy Mater.* **2014**, *4*, 1301857.
(31) Engel, M.; Schaefer, D.; Erni, D.; Benson, N.; Schmechel, R. Reduced Coulomb Interaction in Organic Solar Cells by the Introduction of Inorganic High-k Nanostructured Materials. *Phys. Status Solidi A* **2013**, *210*, 1712−1718.
(32) Germack, D. S.; Chan, C. K.; Kline, R. J.; Fischer, D. A.; Gundlach, D. J.; Toney, M. F.; Richter, L. J.; DeLongchamp, D. M. Interfacial Segregation in Polymer/Fullerene Blend Films for Photovoltaic Devices. *Macromolecules* **2010**, *43*, 3828−3836.
(33) Ashraf, A.; Dissanayake, D. M. N. M.; Germack, D. S.; Weiland, C.; Eisaman, M. D. Confinement-Induced Reduction in Phase Segregation and Interchain Disorder in Bulk Heterojunction Films. *ACS Nano* **2014**, *8*, 323−331.
(34) Aspnes, D.; Theeten, J.; Hottier, F. Investigation of Effective-Medium Models of Microscopic Surface Roughness by Spectroscopic Ellipsometry. *Phys. Rev. B* **1979**, *20*, 3292−3302.
(35) Franta, D.; Ohlídal, I. Comparison of Effective Medium Approximation and Rayleigh−Rice Theory Concerning Ellipsometric Characterization of Rough Surfaces. *Opt. Commun.* **2005**, *248*, 459−467.
(36) Honig, B.; Nicholls, A. Classical Electrostatics in Biology and Chemistry. *Science* **1995**, *268*, 1144−1149.

DOI: 10.1021/acsami.5b01606
ACS Appl. Mater. Interfaces 2015, 7, 11881−11889

(37) Jackson, J. D. *Classical Electrodynamics*, 3rd ed.; Wiley: New York, 1999.
(38) Lu, B. Z.; Zhou, Y. C.; Holst, M. J.; Mccammon, J. A. Recent Progress in Numerical Methods for the Poisson-Boltzmann Equation in Biophysical Applications. *Comm. Comp. Phys.* **2008**, *3*, 973−1009.
(39) Fedkiw, R. P.; Aslam, T.; Merriman, B.; Osher, S. A Non-Oscillatory Eulerian Approach to Interfaces in Multimaterial Flows (The Ghost Fluid Method). *J. Comput. Phys.* **1999**, *152*, 457−492.
(40) Liu, X. D.; Fedkiw, R. P.; Kang, M. A Boundary Condition Capturing Method for Poisson's Equation on Irregular Domains. *J. Comput. Phys.* **2000**, *160*, 151−178.
(41) Leveque, R. Z.; Li, Z. The Immersed Interface Method for Elliptic Equations with Discontinuous Coefficients and Singular Sources. *SIAM J. Numer. Anal.* **1994**, *31*, 1019−1044.
(42) Zhao, S.; Wei, G. W. High-Order FDTD Methods via Derivative Matching for Maxwell's Equations With Material Interfaces. *J. Comput. Phys.* **2004**, *200*, 60−103.
(43) Zhou, Y. C.; Zhao, S.; Feig, M.; Wei, G. W. High Order Matched Interface and Boundary Method for Elliptic Equations with Discontinuous Coefficients and Singular Sources. *J. Comput. Phys.* **2006**, *213*, 1−30.
(44) Yu, S.; Wei, G. W. Three-Dimensional Matched Interface and Boundary (MIB) Method for Treating Geometric Singularities. *J. Comput. Phys.* **2007**, *227*, 602−632.
(45) Tyagi, S.; Süzen, M.; Sega, M.; Barbosa, M.; Kantorovich, S. S.; Holm, C. An Iterative, Fast, Linear-Scaling Method for Computing Induced Charges on Arbitrary Dielectric Boundaries. *J. Chem. Phys.* **2010**, *132*, 154112.
(46) Wright, M.; Uddin, A. Organic-Inorganic Hybrid Solar Cells: A Comparative Review. *Sol. Energy Mater. Sol. Cells* **2012**, *107*, 87−111.
(47) Němec, H.; Rochford, J.; Taratula, O.; Galoppini, E.; Kužel, P.; Polívka, T.; Yartsev, a.; Sundström, V. Influence of the Electron-Cation Interaction on Electron Mobility in Dye-Sensitized ZnO and TiO_2 Nanocrystals: A Study Using Ultrafast Terahertz Spectroscopy. *Phys. Rev. Lett.* **2010**, *104*, 197401.
(48) Nagata, Y.; Lennartz, C. Atomistic Simulation on Charge Mobility of Amorphous Tris(8-hydroxyquinoline) Aluminum (Alq3): Origin of Poole-Frenkel-Type Behavior. *J. Chem. Phys.* **2008**, *129*, 034709.
(49) Rühle, V.; Lukyanov, A.; May, F.; Schrader, M.; Vehoff, T.; Kirkpatrick, J.; Baumeier, B.; Andrienko, D. Microscopic Simulations of Charge Transport in Disordered Organic Semiconductors. *J. Chem. Theory Comput.* **2011**, *7*, 3335−3345.
(50) Graetzel, M.; Janssen, R. A. J.; Mitzi, D. B.; Sargent, E. H. Materials Interface Engineering for Solution-Processed Photovoltaics. *Nature* **2012**, *488*, 304−312.
(51) Riedel, I.; von Hauff, E.; Parisi, J.; Martín, N.; Giacalone, F.; Dyakonov, V. Diphenylmethanofullerenes: New and Efficient Acceptors in Bulk-Heterojunction Solar Cells. *Adv. Funct. Mater.* **2005**, *15*, 1979−1987.
(52) Ross, R. B.; Cardona, C. M.; Guldi, D. M.; Sankaranarayanan, S. G.; Reese, M. O.; Kopidakis, N.; Peet, J.; Walker, B.; Bazan, G. C.; Van Keuren, E.; Holloway, B. C.; Drees, M. Endohedral Fullerenes for Organic Photovoltaic Devices. *Nat. Mater.* **2009**, *8*, 208−212.
(53) Wu, J.-L.; Chen, F.-C.; Hsiao, Y.-S.; Chien, F.-C.; Chen, P.; Kuo, C.-H.; Huang, M. H.; Hsu, C.-S. Surface Plasmonic Effects of Metallic Nanoparticles on the Performance of Polymer Bulk Heterojunction Solar Cells. *ACS Nano* **2011**, *5*, 959−967.
(54) Morfa, A. J.; Rowlen, K. L.; Reilly, T. H.; Romero, M. J.; van de Lagemaat, J. Plasmon-Enhanced Solar Energy Conversion in Organic Bulk Heterojunction Photovoltaics. *Appl. Phys. Lett.* **2008**, *92*, 013504.
(55) Lee, J.-Y.; Peumans, P. The Origin of Enhanced Optical Absorption in Solar Cells with Metal Nanoparticles Embedded in the Active Layer. *Opt. Express.* **2010**, *18*, 10078−10087.
(56) Huang, Y.-F.; Zhang, Z.-L.; Kang, K.-B.; Zhao, M.; Wen, T.; Liu, Y.-X.; Zhai, X.-P.; Lv, S.-K.; Wang, Q.; Qiu, W.-Y.; Qiu, D. Mitigation of Metal-Mediated Losses by Coating Au Nanoparticles with Dielectric Layer in Plasmonic Solar Cells. *RSC Adv.* **2013**, *3*, 16080.
(57) Fabregat-Santiago, F.; García-Cañadas, J.; Palomares, E.; Clifford, J. N.; Haque, S. A.; Durrant, J. R.; Garcia-Belmonte, G.; Bisquert, J. The Origin of Slow Electron Recombination Processes in Dye-Sensitized Solar Cells with Alumina Barrier Coatings. *J. Appl. Phys.* **2004**, *96*, 6903.

DOI: 10.1021/acsami.5b01606
ACS Appl. Mater. Interfaces 2015, 7, 11881−11889